Thermodynamic and Structural Features of Aqueous Ce(III)

Adriana Dinescu and Aurora E. Clark*

Idaho National Laboratory, P.O. Box 1625, Idaho Falls, Idaho 83415-2208, and Department of Chemistry, Washington State University, P.O. Box 644630, Pullman, Washington

Received: August 27, 2008

With a single f-electron, Ce(III) is the simplest test case for benchmarking the thermodynamic and structural properties of hydrated Ln(III) against varying density functionals and reaction field models, in addition to determining the importance of multiconfigurational character in their wave functions. Here, the electronic structure of $Ce(H_2O)_x(H_2O)_y^{3+}$ ($x = 8, 9$; $y = 0, 12-14$) has been examined using DFT and CASSCF calculations. The latter confirmed that the wave function of octa- and nona-aqua Ce(III) is well-described by a single configuration. Benchmarking was performed for density functionals, reaction field cavity types, and solvation reactions against the experimental free energy of hydration, $\Delta G_{hyd}(Ce^{3+})$. The UA0, UAKS, Pauling, and UFF polarized continuum model cavities displayed different performance, depending on whether one or two hydration shells were examined, and as a function of the size of the metal basis set. These results were essentially independent of the density functional employed. Using these benchmarks, the free energy for water exchange between CN = 8 and CN = 9, for which no experimental data are available, was estimated to be approximately −4 kcal/mol.

Introduction

The aqueous chemistry of Ce(III) has relevance to a variety of fields, with the most evident being biomedical imaging and the reprocessing of spent nuclear material. In the former, it is widely known that free Ce(III) is moderately toxic, and thus, a prerequisite for in vivo applications is its complexation with a polydentate ligand to form a compound of high kinetic and thermodynamic stability. In the latter, complexation with a polydentate ligand is also needed for separations purposes, as the Ce-144 isotope is a fission product from the nuclear fuel cycle and is a constituent in high-level radioactive waste due to its strong γ-ray decay.[1] Though its short half-life (285 days) prevents Ce-144 from being a long-term environmental hazard, the potential closure of the nuclear fuel cycle proposes liquid/liquid extraction techniques for separating both 4f and 5f elements, and thus its complexation chemistry gains importance. Regardless of the eventual application of the Ce(III) complexes, mechanisms for ligand binding (associative vs dissociative) will be significantly influenced by the strength of the M-OH_2 interaction and the extent of water organization about the ion. Within the alkali and alkaline earth series, the metal−water interaction is exclusively ionic in character, while transition metal aquo complexes have coordination geometries that are strongly dependent upon the metal electronic state due to the participation of the d-orbitals in the M-OH_2 bond.[2] Among the lanthanide (Ln) elements, it is possible for the 4f orbitals to participate in bonding, but in a manner likely dependent upon the position of the element within the period (correlating to the importance of relativistic effects) and its oxidation state. The extent to which the Ln 4f electrons participate in bonding is often debated within the literature. While most studies indicate that the 4f orbitals/electrons do not participate in bonding, some systems (e.g., lanthanide trihalides) have shown pronounced 4f hybridization indicative of covalent bonding interactions.[3]

The inner coordination sphere of aqueous Ln(III) is known to be dynamic, with significant exchange of the first- and second-shell H_2O being possible.[4] Experimentally, it is well-established that early Ln(III) form nona-aqua inner-sphere complexes in aqueous solution, while late Ln(III) form octa-aqua complexes. Molecular dynamics simulations of water exchange between the first and second coordination shells of La^{3+} and Eu^{3+} also confirm that La^{3+} prefers a 9-coordinate arrangement (92% for CN = 9 and 8% for CN = 8) while an equilibrium between 9- and 8-coordinate was detected for Eu^{3+} (37% for CN = 9 and 63% for CN = 8).[5] Given the increasing use of computational methods (e.g., density functional theory - DFT) to study trivalent Ln, and the relative "weakness" of the Ln-OH_2 interaction in the aqueous phase, it is imperative that benchmarks are performed to elucidate the most appropriate density functionals, basis sets, and electronic structure analysis methods to be used. In a recent study, we examined the role of density functionals and basis sets upon the structural parameters of closed-shell $La(H_2O)_{8,9}^{3+}$ and $Lu(H_2O)_8^{3+}$.[6a] Here, we seek to assess which methods are appropriate for determining the thermodynamics of solvation for Ln(III), with an emphasis upon taking into account the appropriate potential multiconfigurational character of open-shell trivalent species. Ce(III) is computationally the most simple trivalent lanthanide to study due to its single f-electron.

Computational Methods

All calculations were performed with the *NWChem*[7] and *Gaussian03*[8] packages. The B3LYP[9] hybrid exchange-correlation functional was first employed to optimize the equilibrium geometries of $Ce(H_2O)_8^{3+}$, $Ce(H_2O)_8(H_2O)_{14}^{3+}$, $Ce(H_2O)_9^{3+}$, and $Ce(H_2O)_9(H_2O)_{12-14}^{3+}$ complexes and $(H_2O)_{8-9}$ and $(H_2O)_{21-22}$ water cluster molecules. Frequency calculations were performed to obtain thermochemical corrections and ensure that all structures were local minima (no imaginary vibrations). The optimized $Ce(H_2O)_8^{3+}$ and $Ce(H_2O)_9^{3+}$ geometries obtained from the Jacob's ladder of DFT functionals,[10] including LSDA

* Author to whom correspondence should be addressed: auclark@wsu.edu.

10.1021/jp8076408 CCC: $40.75
Published on Web 10/10/2008

(SVWN[11]), GGA (PW91[12]), hybrid (B3LYP), and meta-GGA (TPSS[13]) functionals were also compared. Geometry optimizations in *NWChem* employed an SCF energy convergence criterion of 10^{-6}, an integral internal screening threshold of 10^{-16}, a numerical integration grid of 10^{-8}, and a tolerance in Schwarz screening for the Coulomb integrals of 10^{-12}. Geometry optimizations of the water clusters were performed with *Gaussian03* and employed an SCF energy convergence of 10^{-6} and an Ultrafine grid for numerical integration. No symmetry constraints have been imposed during the optimizations. The Stuttgart "small-core" RSC28[14] segmented and "large-core" RLC47[15] effective core potentials (ECP) were utilized for the Ce(III) cation, where 28 and 47 inner-shell electrons, respectively, are replaced by pseudopotentials that account for scalar relativistic effects (these are the electrons associated with the $1s^22s^22p^63s^23p^63d^{10}$ and $1s^22s^22p^63s^23p^63d^{10}4s^24p^64d^{10}4f^1$ core electronic configurations, respectively). The most diffuse s function was omitted from the Ce RSC28 basis set due to linear dependency. Given that large-core ECPs place the f-electrons in the core, RLC47 was chosen according to the formal oxidation state of Ce(III). Thus, the [9s,8p,5d,4f,3 g] basis describes the $4s^24p^65s^24d^{10}5p^64f^1$valence electrons of Ce in the small-core calculation, while the [5s,4p,3d] basis describes the $5s^25p^6$ valence electrons in the large-core calculations. All H and O atoms employed the aug-cc-pVDZ basis set.[16] To analyze the electronic structure, a modified natural population analysis[6] (NPA) was performed, which has the 6s6p5d4f natural atomic orbitals (NAOs) within the valence space. Different valence electron configurations have been examined utilizing molecular orbital swapping within the f-orbital framework. Single-point second-order Moller−Plessett (MP2)[17] perturbation theory calculations at the optimized B3LYP geometries were performed using the Stuttgart RSC28 segmented basis set on Ce(III). The complete active space self-consistent field (CASSCF) method[18] was used to examine the multiconfigurational nature of the $Ce(H_2O)_{8,9}^{3+}$ wave functions. As Ce(III) has a valence electronic configuration of $4f^1$, a minimal active space composed of the one electron in the seven 4f orbitals (1,7) was used. The counterpoise (CP) correction of Boys and Bernardi[19] was employed to evaluate the magnitude of basis set superposition error (BSSE) associated with the addition of one water molecule to the $Ce(H_2O)_8^{3+}$ species. The corrections were applied a posteriori and fragment relaxation energy terms were included in the estimation of BSSE.[20] The hydration free energies of Ce^{3+} were corrected for solvation effects through the use of the polarizable continuum model (PCM)[21] for water. Single-point calculations using SCF energy convergence criteria of 10^{-6} (SCF=TIGHT) were performed at the B3LYP level of theory with various solute cavity models, UA0,[22] UFF,[22] UAHF,[22] UAKS,[22] and partially scaled Pauling[23] radii ($\alpha = 1.1$). *NWChem* calculations were performed on the massively parallel Linux cluster in the Molecular Science Computing Facility in the William R. Wiley Environmental Molecular Sciences Laboratory at the Pacific Northwest National Laboratory or at the National Energy Research Scientific Computing Center (NERSC), a DOE Office of Science user facility at Lawrence Berkeley National Laboratory.

Results and Discussion

$Ce(H_2O)_8^{3+}$and $Ce(H_2O)_9^{3+}$. ***Geometries.*** Representative structures of optimized C_1 gas-phase square antiprismatic $Ce(H_2O)_8^{3+}$ and tricapped trigonal bipyrimidal $Ce(H_2O)_9^{3+}$ are shown in Figure 1, with specific structural parameters discussed in Table 1. In agreement with our previous studies,[6a] we find

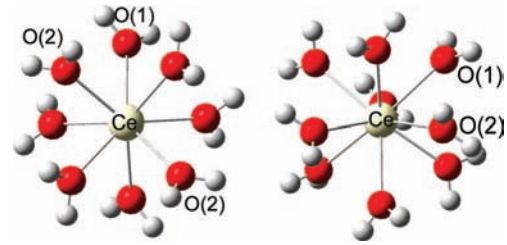

Figure 1. Square antiprismatic $Ce(H_2O)_8^{3+}$ and tricapped trigonal bipyramidal $Ce(H_2O)_9^{3+}$ obtained using DFT. Specific structural parameters with varying density functionals and basis sets in Table 1.

TABLE 1: Structural Parameters of the Primary Coordination Sphere of $Ce(H_2O)_{8,9}^{3+}$,$Ce(H_2O)_8(H_2O)_{14}^{3+}$, and $Ce(H_2O)_9(H_2O)_{12}^{3+}$Obtained with LSDA (SVWN5), GGA (PW91), meta-GGA (TPSS), and Hybrid (B3LYP) Functionals Using the Small- (RSC28) and Large Core (RLC47) RECPs with Their Associated Bases and the aug-cc-PVDZ Basis on O and H[a]

	~symm	tol	$\langle r_{Ce-O(1)}\rangle$	$\langle r_{Ce-O(2)}\rangle$
		$Ce(H_2O)_8^{3+}$		
SVWN5 RSC28	C_2	0.1	2.45474	2.47151
PW91 RSC28	S_8	0.1	2.53347	2.54312
TPSS RSC28	C_2	0.1	2.53328	2.54910
B3LYP RSC28	C_2	0.1	2.54792	2.56579
B3LYP RLC47	S_8, C_4, C_2	0.01	2.58082	[b]
		$Ce(H_2O)_8(H_2O)_{14}^{3+}$		
B3LYP RSC28	C_1		2.50072	2.56860
B3LYP RLC47	C_1		2.54273	2.58579
		$Ce(H_2O)_9^{3+}$		
SVWN5 RSC28	D_3, C_3, C_2	0.1	2.49274	2.50655
PW91 RSC28	D_3, C_3, C_2	0.1	2.56629	2.59574
TPSS RSC28	C_2	0.1	2.56421	2.59285
B3LYP RSC28	C_3	0.1	2.59069	2.59507
B3LYP RLC47	D_3, C_3, C_2	0.01	2.61528	2.62617
Expt.[c]			2.52	2.52
		$Ce(H_2O)_9(H_2O)_{12}^{3+}$		
B3LYP RSC28	C_1		2.55281	2.62454
B3LYP RLC47	C_1		2.57682	2.65097

[a] Nearest symmetry group (Symm), tolerance to reach higher symmetry (Tol), and average bond lengths $\langle r_{Ce-O}\rangle$ in Å, with oxygens as labeled in Figure 1 are presented. [b] In this case O(1)=O(2). [c] ref 26.

that the smallest M-OH_2 bond lengths are obtained with LSDA, while GGA and meta-GGA functionals yield nearly identical M-OH_2 bond lengths and B3LYP predicts the longest Ce-OH_2 values. Use of the Stuttgart RLC47 basis lengthens the Ce−O bond lengths in both the 8- and 9-coordinate species for each bond by ~0.03 Å, with more symmetry also being observed (see Supporting Information). This result is consistent with the expected performance of large-core pseudopotentials, which presumably overestimate the metal−ligand bond lengths due to poorer treatment of the core−valence correlation relative to the small-core calculations.[24] However, it is also possible that the large-core structures could be significantly improved by extending the structure to include a second hydration shell (vide infra). Within the small-core B3LYP calculations, increasing the hydration number from eight to nine increases the bond length by up to 0.03 Å, in addition to decreasing the metal charge by 0.1 e^- (as calculated by NPA). The water molecules of the first hydration shell form eight hydrogen bonds in the $Ce(H_2O)_8^{3+}$ species, while the $Ce(H_2O)_9^{3+}$ complex is stabilized by twelve hydrogen bonds (see Supporting Information). Experimentally, several solid-state X-ray structures[25] of the

primary coordination shell of hydrated Ce^{3+} indicate a 9-coordinate species. Unfortunately, a wide range of solid-state Ce-OH_2 bond lengths are reported for nona-aqua Ce(III) depending on the counterion in the crystal. Lanthanide nona-aqua complexes can range from tricapped trigonal bipyramidal (TTB) of D_{3h} symmetry to monocapped square antiprisms of C_4 symmetry. In the case of $Ce(H_2O)_9^{3+}$, all reported species are TTB, with shorter prismatic Ce-OH_2 distances, than equatorial Ce-OH_2 bonds. Experimentally, $Ce(H_2O)_9^{3+}$ using ethyl sulfate or toluene-4-sulfonate as a counterion results in slightly distorted TTBʼs of C_{3h} symmetry. In the former, reported Ce−O bond lengths for the prismatic bonds are 2.491 Å, while the equatorial bond lengths are 2.600 Å.[25b] In the latter, the prismatic bonds are 2.489 Å and the equatorial bond lengths are 2.534 Å.[25e] EXAFS data[26] for Ce(III) in dilute chloride solutions support a 9-coordinate inner hydration sphere (CN = 9.3) with average Ce-OH_2 bond lengths of 2.52 Å reported. Given the large variation in bond lengths, it is difficult to assess the density functional performance with respect to structural parameters when only a primary hydration shell is present. While GGA, meta-GGA, and B3LYP with a small-core RESCP each yield Ce-OH_2 bond lengths for the prismatic ligating waters that are in good agreement with a variety of solid-state $Ce(H_2O)_9^{3+}$ structures, none of the functionals predict lengthening of the equatorial Ce-OH_2 bonds of more than 0.03 Å, which is a smaller perturbation than generally experimentally observed. Comparison of the experimental solution phase (which is an average over all Ce-OH_2 bond lengths) and theoretical gas-phase data shows the best structural agreement using TPSS (a meta-GGA functional), followed by PW91 and then B3LYP. Interestingly, inclusion of a second hydration shell (vide infra) does lead to structures (using B3LYP) that have significant lengthening of the equatorial bonds (by ∼0.07 Å), and thus the discrepancy relative to experiment appears to derive from the lack of the second-shell waters.

Electronic Structure. While previous studies have indicated that strongly bound Ce(III) complexes, like Cp_2CeI, have wave functions that are to a good approximation a single configuration,[27] water is a weak crystal field splitting ligand, which may lead to small energy differences between electronic states with different f-electron occupations. To investigate the most appropriate description of hydrated Ce(III), we have examined: (1) different "single determinant"[28] doublet electronic states obtained using DFT (Δ-SCF method), and (2) the lowest energy state using CASSCF, which determines if excited-state determinants within the active space make significant contributions to the wave function beyond the HF reference.

First, let us consider the electronic structure of the C_1 B3LYP $Ce(H_2O)_8^{3+}$ and $Ce(H_2O)_9^{3+}$ species. Examination of the natural orbitals obtained by Lowdin orthogonalization[29] of the C_1 molecular orbitals indicates that the singly occupied Kohn−Sham orbital of f-character is quite mixed, with large contributions from the f_{z^3}, f_{xz^2}, and f_{xyz} atomic orbitals in $Ce(H_2O)_8^{3+}$ and the f_{z^2}, f_{xyz}, and $f_{z(3x^2-y^2)}$ atomic orbitals in $Ce(H_2O)_9^{3+}$ (Figure 2). Natural bond order analysis, which examines the bonding behavior in analogy to the Lowdin orbitals, found no covalent bonding interactions between the Ce and OH_2 units. Utilizing the natural orbitals as an initial guess, we performed (1,1) CAS calculations (1 electron in 1 f-orbital) at the C_1 B3LYP optimized geometries of $Ce(H_2O)_{8-9}^{3+}$. A (1,1) CASSCF is equivalent to an ROHF calculation and allowed the determination of the total electronic energy of each structure without any correlation caused by excited-state mixing in the wave function. A (1,7) CASSCF calculation was then performed,

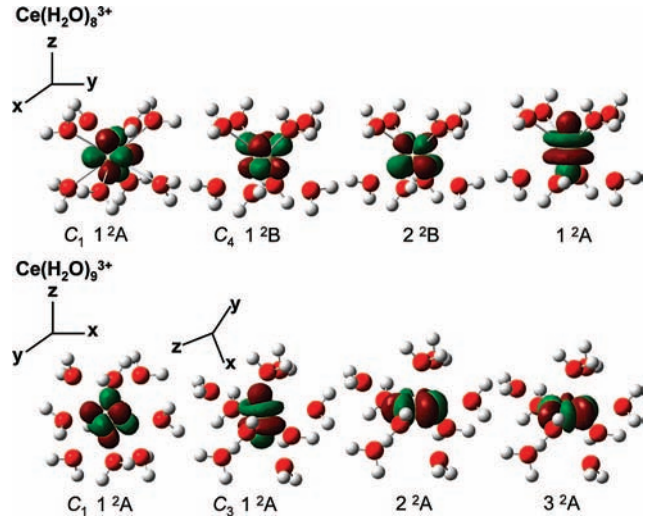

Figure 2. Singly occupied Kohn−Sham B3LYP orbitals for the lowest-energy 1 ^{2}A state of the C_1 optimized structures, and the three lowest-energy electronic states at the symmetrized C_4 structure of $Ce(H_2O)_8^{3+}$ and C_3 structure of $Ce(H_2O)_9^{3+}$, respectively.

which allowed all potential electronic excitations of the single electron in each of the seven 4f orbitals. In the case of $Ce(H_2O)_8^{3+}$, the (1,1) and (1,7) CASSCF total ground-state electronic energies differed by less than 0.0001 millihartrees and the (1,7) wave function consisted of a single configuration with a coefficient of 0.99998. Similar results were obtained for $Ce(H_2O)_9^{3+}$. Thus, the wave functions of $Ce(H_2O)_{8-9}^{3+}$ are well-represented by a single configuration and should be adequately described by DFT. Further, the singly occupied Lowdin natural orbitals for both the (1,1) and (1,7) CASSCF of $Ce(H_2O)_8^{3+}$ show significant mixing of the 4f orbitals, similar to that observed in the singly occupied KS orbital from B3LYP.

Owing to the computational expense of the CASSCF calculations and the clear single determinant character of the ground state, we determined explicit excited doublet states of the hydrated Ce^{3+} clusters. Spin−orbit (SO) coupling was ignored; however, it is known for bare Ce^{3+} ion that calculated SO coupling constants are 600−700 cm^{-1}.[29c] The small-core C_1 optimized geometries of $Ce(H_2O)_8^{3+}$ and $Ce(H_2O)_9^{3+}$ were first symmetrized to C_4 and C_3, respectively. B3LYP single-point energy calculations performed on the symmetric structures reveal that these structural modifications increase the total electronic energy of $Ce(H_2O)_8^{3+}$ by 3.33 kcal/mol and of $Ce(H_2O)_9^{3+}$ by 2.80 kcal/mol. The lowest-energy doublet state of C_4 $Ce(H_2O)_8^{3+}$ is the 1 ^{2}B, which has occupation of the $f_{z(x^2-y^2)}$ (Table 2; Figure 2). Using the Δ-SCF method, two other states, the 2 ^{2}B (f^1_{xyz}) and 1 ^{2}A ($f^1_{z^3}$) were found to be nearly degenerate. Electronic states with occupation of the remaining f-orbitals are likely much higher in energy owing to their repulsive interactions of the lone electron with the oxygen lone pair orbitals of the ligating waters. Only one of these states was able to be determined using B3LYP Δ-SCF, the 1 ^{2}E ($f^1_{y(3x^2-y^2)}$), which is 37.02 kcal/mol higher in energy than the ground state.

The singly occupied orbitals for the lowest-energy doublet states in the nine-coordinate species differ from those of the octa-aqua system owing to the change from the square antiprismatic to tricapped trigonal bipyramidal geometry and minimization of electrostatic repulsion between the water lone pair orbitals and the singly occupied f-orbital. The lowest-energy doublet state of C_3 $Ce(H_2O)_9^{3+}$ is the 1 ^{2}A, which has occupation of the f_{z^3} (Table 2; Figure 2). Using the Δ-SCF method, two states, the 2 ^{2}A ($f^1_{x(x^2-3y^2)}$) and the 3 ^{2}A ($f^1_{y(3x^2-y^2)}$) are within 2

TABLE 2: Gas-Phase Δ-SCF B3LYP/RSC28/aug-cc-pVDZ Electronic Energies of the C_4 $Ce(H_2O)_8^{3+}$ and C_3 $Ce(H_2O)_9^{3+}$structures[a]

$Ce(H_2O)_8^{3+}$			$Ce(H_2O)_9^{3+}$		
state/occupation	$E_{elec.}$	relative E	state/occupation	$E_{elec.}$	relative E
$^2B/f^1_{z(x^2-y^2)}$ ($m_l = 2$)	−1085.964798	0.00	$^2A/f^1_{z^3}$ ($m_l = 0$)	−1162.449026	0.00
$^2B/f^1_{xyz}$ ($m_l = -2$)	−1085.964768	0.02	$^2A/f^1_{x(x^2-3y^2)}$ ($m_l = 3$)	−1162.447893	0.71
$^2A/f^1_{z^3}$ ($m_l = 0$)	−1085.964165	0.40	$^2A/f^1_{y(3x^2-y^2)}$ ($m_l = -3$)	−1162.445388	2.28
$^2E/f^1_{y(3x^2-y^2)}$ ($m_l = -3$)	−1085.905800	37.02	$^2E/f^1_{yx^2}$ ($m_l = -1$)	−1162.402774	29.02

[a] Total electronic energy, E_{elec}, in hartree (1 hartree = 627.5 kcal/mol); relative energy in kcal/mol.

TABLE 3: Gas-Phase Energetics (kcal/mol) for Reaction 1 Using the C_1 Structures of $Ce(H_2O)_8^{3+}$ and $Ce(H_2O)_9^{3+}$[a]

level	$\Delta E_{elec.}$	ΔE_{ZPE} (298.15 K)	ΔH (298.15 K)	$-T\Delta S$ (298.15 K)	ΔG (298.15 K)
SVWN5/RSC28	−30.85	−28.25	−28.84	12.09	−16.75
PW91/RSC28	−22.73	−19.98	−20.57	12.08	−8.49
TPSS/RSC28	−23.96	−21.62	−22.21	7.89	−14.32
B3LYP/RSC28	−22.43	−20.61	−21.20	10.57	−10.64
B3LYP/RSC28[b,c]	−22.96		−21.73[d]		−11.16[d]
B3LYP/RLC47	−22.80	−20.46	−21.05	10.65	−10.40
MP2/RSC28[d]	−27.88		−26.65[d]		−16.08[d]

[a] Zero point energy (ZPE) and thermal corrections (298.15 K) are included, in addition to the B3LYP change in the total electronic energetics of the symmetrized structures. [b] Single point calculation on the symmetrized C_4 structure of $Ce(H_2O)_8^{3+}$ and C_3 structure of $Ce(H_2O)_9^{3+}$. [c] The f orbital occupations for $Ce(H_2O)_8^{3+}$ and $Ce(H_2O)_9^{3+}$ were $f^1_{z^3}$ ($m_l = 0$) and $f^1_{y(3x^2-y^2)}$ ($m_l = -3$), respectively. [d] Single point calculation with B3LYP/RSC28/aug-cc-pVDZ thermochemistry corrections and entropy change for the C_1 symmetry.

TABLE 4: Thermodynamic Properties of Reaction 1 in Aqueous Solution (kcal/mol) at the B3LYP/RSC28/aug-cc-pVDZ Level Using Various PCM Cavities[a,b]

PCM cavity	ΔH (298.15 K)	ΔG (298.15 K)	$\Delta\Delta G_{solv}$ (elec.)	$\Delta\Delta G_{solv}$ (nonelec.)	$\Delta\Delta G_{solv}$ (tot.)	SS corr.	$\Delta G_{corr.}$
UA0	−21.20	−10.64	13.26	−2.63	10.64	−4.3	−4.29
UFF	−21.20	−10.64	14.42	−2.14	12.29	−4.3	−2.64
UAHF, UAKS	−21.20	−10.64	12.21	−1.43	10.78	−4.3	−4.15
Pauling, α = 1.1	−21.20	−10.64	18.81	2.40	21.21	−4.3	6.28

[a] PCM calculations were performed with *Gaussian03* code using the gas-phase optimized C_1 geometries of $Ce(H_2O)_8^{3+}$ and $Ce(H_2O)_9^{3+}$. [b] Scaled UAHF and UAKS radii (scaling factor = 1.2) were used.

kcal/mol of the ground state. Occupation of the f_{yz^2}, f_{xz^2}, f_{xyz}, or $f_{z(x^2-y^2)}$ orbitals likely leads to high-energy states like the 1 ^2E ($f^1_{yz^2}$) whose lone electron has large repulsion with H_2O, causing it to be 29.02 kcal/mol higher in energy than the ground state according to Δ-SCF. Both the doublet E states in the 8- and 9-coordinate species are also susceptible to Jahn−Teller distortion, and thus, their single-point energies at the ground-state geometries are likely to be abnormally high. Further, this electronic description provided in these Δ-SCF calculations did not significantly deviate among all of the functionals examined.

Water Exchange Reactions: Part I. ***Gas-Phase Results.*** While the crystal structures of hydrated Ce^{3+} reveals a 9-coordinate geometry,[25] water exchange will lead to some presence of the 8-coordinate species in aqueous solution. To assess the preference of $Ce(H_2O)_9^{3+}$ over $Ce(H_2O)_8^{3+}$, we first investigated the gas-phase energetics of reaction 1. The gas-phase energies, enthalpies, and Gibbs free energies for this reaction at different levels of theory are provided in Table 3.

$$Ce(H_2O)_8^{3+} + H_2O \rightarrow Ce(H_2O)_9^{3+} \quad (1)$$

In agreement with experimental observations, each functional predicts that the addition of water to the 8-coordinate species is exothermic. Overall, a broad range of free energies of reaction are observed, spanning approximately 8 kcal/mol. LSDA and MP2 (at the B3LYP geometry) predict a large negative value for ΔG at nearly −17 kcal/mol. The PW91 GGA functional predicts the free energy of reaction to be −8.49 kcal/mol, which is reasonably close to the value predicted by hybrid B3LYP. The meta-GGA functional TPSS yields free energies between the LSDA and GGA/hybrid methods. Use of a small-core versus large-core basis does not influence the C_1 predicted energies of reaction beyond the anticipated chemical accuracy of DFT. Imposition of symmetry causes the gas-phase reaction energies to become slightly more negative in the small-core basis. It is important to note that the calculation of reaction 1 energetics is subject to basis set superposition error (BSSE) due to the incompleteness of the basis sets utilized in this work. To estimate the extent of BSSE at the B3LYP/RSC28 level, we have employed the commonly used counterpoise correction.[19] We have applied this method as a single-point correction to previously optimized geometries using Xantheas' scheme.[20] Fragments in the $Ce(H_2O)_9^{3+}$ molecule are as follows: (1) the water ligand with the longest Ce−O bond distance and (2) the remaining $Ce(H_2O)_8^{3+}$ fragment. The calculated BSSE for the electronic energy of reaction 1 is only 1.54 kcal/mol, making the corrected B3LYP/RSC28 binding energy ΔE (BSSE) = −21.26 kcal/mol.

Solvent Phase Models. To take into account solvent affects upon reaction 1, we have examined different implementations of the polarized continuum model (PCM),[21] which to first order accounts for the interaction of the dielectric of the solvent with the hydrated Ce(III) solute. Few PCM studies of f-elements have been performed; however, Gutowski et al. examined several cavity models for the water addition reaction to the tetra-aquo uranyl cation using both PCM and CPCM approaches.[30] There, partially scaled (α = 1.1) Pauling radii and unscaled UAKS and UAHF radii yielded results consistent with experimental values (within 1 kcal/mol). Table 4 contains the electrostatic

and nonelectrostatic contributions of solvation to the free energy of reaction 1 as a function of the solute cavity model, as well as the standard-state thermodynamic correction (SS corr.) of $-4.3/n$ kcal/mol for each $(H_2O)_n$ water cluster using the B3LYP functional.[30,31] The free energy of reaction in aqueous solution can be defined as

$$\Delta G_{\text{corr.}} = \Delta G_{\text{gas}}^{298.15} + \Delta\Delta G_{\text{solv}}^{\text{tot}} + \text{SS}^{\text{corr}} \quad (2)$$

where $\Delta G_{\text{gas}}{}^{298.15}$ is the free energy of reaction in the gas phase, $\Delta\Delta G_{\text{solv}}{}^{\text{tot}}$ is the solvation contribution to the free energy of reaction, and SS^{corr} is the standard-state thermodynamic correction. In PCM, the solvation contribution to the free energy of a molecule can be expressed

$$\Delta G_{\text{solv}}^{\text{tot}} = \Delta G_{\text{solv}}^{\text{elec}} + \Delta G_{\text{solv}}^{\text{nonelec}} \quad (3)$$

where $\Delta G_{\text{solv}}{}^{\text{elec}}$ is the electrostatic component of $\Delta G_{\text{solv}}{}^{\text{tot}}$, while $\Delta G_{\text{solv}}{}^{\text{nonelec}}$ is the sum of the nonelectrostatic components of the $\Delta G_{\text{solv}}{}^{\text{tot}}$. For reaction 1, eq 3 can be written

$$\Delta\Delta G_{\text{solv}}^{\text{tot}} = \Delta\Delta G_{\text{solv}}^{\text{elec}} + \Delta\Delta G_{\text{solv}}^{\text{nonelec}} \quad (4)$$

where

$$\Delta\Delta G_{\text{solv}} = \Delta G_{\text{solv}}(\text{Ce}(\text{H}_2\text{O})_9{}^{3+}) - [\Delta G_{\text{solv}}(\text{Ce}(\text{H}_2\text{O})_8{}^{3+}) + \Delta G_{\text{solv}}(\text{H}_2\text{O})] \quad (5)$$

As in previous studies, our results highlight that PCM corrections are highly dependent on the choice of cavity model and yield more positive free energies of reaction than the gas phase due to the positive contribution of solvation energy. The calculated cavity volumes and surface areas for both $Ce(H_2O)_8{}^{3+}$ and $Ce(H_2O)_9{}^{3+}$ species are presented in the Supporting Information. Our results are equivalent for UAHF and UAKS radii, reflected in both the size of the cavity and energy calculations. While the corrected free energy, $\Delta G_{\text{corr.}}$, remains negative when using the UA0, UFF, and UAHF/UAKS cavities, employing different cavities like the partially scaled Pauling (scaling factor = 1.1) cavities, can alter reaction 1 from the experimentally known exergonic to endergonic.

These results are in contrast to the previous uranyl studies that recommended the use of relatively small cavities.[30] In our study, the smallest cavity (Pauling radii scaled by 1.1) yields a chemically unreasonable endergonic ΔG. Further, we find that the values of ΔG do not correlate well with the cavity size. While smaller positive contributions to the free energy of reaction in aqueous solution are generally given by larger cavities (UA0, UFF, UAHF, and UAKS), this trend is not an absolute. Indeed, the largest cavities of the aqua cerium ions (generated by UFF radii, Supporting Information) do not yield the least positive $\Delta\Delta G_{\text{solv}}$ for reaction 1. This observation suggests that, besides the cavity size, the cavity shape may also be important within the PCM model, a feature that may be enhanced in the solvation of hard-sphere 3+ cations, which have much less directed water ligation relative to the linear dioxo uranyl 2+ cations studied previously.

The large variation in the gas-phase addition reaction energetics (depending on density functional) and the extreme deviation in thermodynamic values as a function of PCM cavity type, in combination with the lack of experimental data, make it imperative to benchmark both functional and cavity against an experimentally known quantity, such as the free energy of hydration. This benchmarking will allow the determination of chemically reasonable thermodynamic values of reaction 1.

Benchmarking Ce^{3+} Hydration Thermodynamics. ***Performance of PCM Models.*** In this section, the influence of bulk solvent effects on the free energy of hydration of Ce^{3+} ion is analyzed. Studies have demonstrated that, unlike the exchange energies, the hydration free energy of an ion can be accurately predicted when the inner solvation shell is treated quantum mechanically and the bulk solvent is approximated by a continuum model.[32] More recently, it has been shown that a single coordination shell combined with a continuum model is adequate to predict the free energy of solvation of the uranyl cation.[30] On the basis of these studies and possible coordination numbers of Ce^{3+} in solution, we have included eight and nine water molecules in the first hydration shell, respectively. Aqueous free energy corrections were calculated using the PCM approach[21] with the B3LYP functionals and both the small- and large-core RECPs. As the PCM implementation is directly determined by solute cavity type, we have tested various models. In previous studies, Consentino et al. found that UATM[22] (UAHF in *Gaussian03*) atomic radii coupled with CPCM[33] reproduce the experimental hydration free energies for all trivalent cations in the lanthanide series.[34] Consistent with the implementation of UAHF radii, the UATM radii were scaled by 1.2 in the calculations of electrostatic contributions, while the calculations of nonelectrostatic contributions employed the unscaled values. Yet, their calculations for the whole lanthanide series employed large-core ECPs with $46 + 4f^n$ electrons in the core and did not explicitly include the first hydration shell. Further, these authors adjusted the experimental references for the hydration free energies based on an updated $\Delta G^0{}_{\text{hyd}}(H^+)$ value of -264.0 kcal/mol,[35] while most references are based on a $\Delta G^0{}_{\text{hyd}}(H^+)$ value of -254.8 kcal/mol. Consequently, they used a $\Delta G^0{}_{\text{hyd}}(Ce^{3+})$ value of -802.4 kcal/mol as an experimental reference. Recently, there has been a large consensus regarding the updated value of $\Delta G^0{}_{\text{hyd}}(H^+)$.[36] Several experimental values have been reported for Ce^{3+} hydration. Morss[37] reported in 1971 a hydration enthalpy value of -805.1 kcal/mol. In 1977, Gomer and Tryson[38] reported a free energy of solvation of -786.3 kcal/mol that used standard half-cell potentials for calculating single ion free energies of solvation. More recently, based on the values calculated by Bratsch and Lagowski,[39] Rizkalla and Choppin[40] reported a hydration enthalpy of -807.84 kcal/mol and a free energy of hydration of -774.2 kcal/mol (this value has an expected error of *ca.* ± 11 kcal/mol due to uncertainties in the reference-state values of hydration of H^+).

To further examine the effectiveness of different solvation models for hydration of the Ce^{3+} ion, we have investigated the thermodynamics of the following reactions (Table 5):

$$\text{Ce}_{(\text{gas})}{}^{3+} + (\text{H}_2\text{O})_{8(\text{aq})} \rightarrow \text{Ce}(\text{H}_2\text{O})_8{}^{3+}{}_{(\text{aq})} \quad (6)$$

$$\text{Ce}_{(\text{gas})}{}^{3+} + 8\text{H}_2\text{O}_{(\text{aq})} \rightarrow \text{Ce}(\text{H}_2\text{O})_8{}^{3+}{}_{(\text{aq})} \quad (7)$$

$$\text{Ce}_{(\text{gas})}{}^{3+} + (\text{H}_2\text{O})_{9(\text{aq})} \rightarrow \text{Ce}(\text{H}_2\text{O})_9{}^{3+}{}_{(\text{aq})} \quad (8)$$

$$\text{Ce}_{(\text{gas})}{}^{3+} + 9\text{H}_2\text{O}_{(\text{aq})} \rightarrow \text{Ce}(\text{H}_2\text{O})_9{}^{3+}{}_{(\text{aq})} \quad (9)$$

Both water clusters (reactions 6 and 8) and discrete water molecules (reactions 7 and 9) have been examined, although the results of the reactions 7 and 9 should be regarded as less reliable, since there is a significant imbalance in the number of particles on the reactant and product sides of the reaction (see Supporting Information). The entropy penalty caused by this imbalance is partially recovered by applying the standard-state correction. The water cluster models used in reactions 6 and 8 minimize the unfavorable entropy changes seen in reactions 7

TABLE 5: Free Energy of Ce^{3+} Hydration (kcal/mol) Using PCM[a] with Different Cavities, And with Different Gas-Phase Solvation Models (Reactions 6 and 8) at B3LYP Level with Small- and Large-Core RECPs and the aug-cc-PVDZ Basis for O and H (Thermodynamic Values for Reactions 7 and 9 Given in *Supporting Information*)

rxn	PCM cavity	ΔG (298.15 K)	$\Delta\Delta G_{solv}$ (electrostatic)	$\Delta\Delta G_{solv}$ (nonelec.)	$\Delta\Delta G_{solv}$ (tot.)	SS corr.	ΔG_{corr}	expt.
			B3LYP/RSC28/aug-cc-PVDZ Level					
6	UA0	−402.67	−376.67	−2.62	−379.29	−0.54	−782.49	−786.3[b]
8	UA0	−412.76	−372.20	−4.05	−376.26	−0.48	−789.49	−774.2[c]
6	UFF	−402.67	−345.81	7.68	−338.13	−0.54	−741.33	
8	UFF	−412.76	−338.07	7.00	−331.08	−0.48	−744.31	
6	UAHF, UAKS	−402.67	−366.56	−0.66	−367.22	−0.54	−770.42	
8	UAHF, UAKS	−412.76	−362.03	−2.66	−364.70	−0.48	−777.93	
6	Pauling, $\alpha = 1.1$	−402.67	−371.91	8.94	−362.97	−0.54	−766.17	
8	Pauling, $\alpha = 1.1$	−412.76	−362.18	10.86	−351.32	−0.48	−764.55	
			B3LYP/RLC47/aug-cc-PVDZ Level					
6	UA0	−384.00	−374.84	−2.22	−377.06	−0.54	−761.60	
8	UA0	−393.85	−370.58	−3.61	−374.20	−0.48	−768.53	
6	UFF	−384.00	−344.66	8.31	−336.34	−0.54	−720.88	
8	UFF	−393.85	−336.76	7.55	−329.22	−0.48	−723.55	
6	UAHF, UAKS	−384.00	−364.83	−0.01	−364.84	−0.54	−749.38	
8	UAHF, UAKS	−393.85	−360.48	−2.05	−362.55	−0.48	−756.88	
6	Pauling, $\alpha = 1.1$	−384.00	−371.72	9.18	−362.54	−0.54	−747.08	
8	Pauling, $\alpha = 1.1$	−393.85	−360.70	11.13	−349.56	−0.48	−743.89	

[a] PCM calculations were performed with *Gaussian03* code using the gas-phase optimized geometries of $Ce(H_2O)_8^{3+}$, $Ce(H_2O)_9^{3+}$, $(H_2O)_8$, and $(H_2O)_9$. Note that slight deviations in energy may occur, relative to the gas-phase *NWChem* calculations, owing to the fact that the implementation of B3LYP in G03 uses the VWN3 functional for local correlation, while B3LYP in *NWChem* uses VWN1RPA. [b] ref 38. [c] ref 40.

and 9, and provide a better description by maintaining the hydrogen bonding network in both sides of reaction.

Our results for reactions 6−9 are not consistent with the calculated value of Consentino et al., who reported a $\Delta G^0_{hyd}(Ce^{3+})$ of −804.5 kcal/mol with the mPW1PW functional and UATM cavities.[34] These differences are likely caused by the fact that we have included the first hydration shell in the QM calculation in addition to the bulk solvent effects. Indeed, comparison of the single-point $Ce(H_2O)_9^{3+}$ result from the UAHF calculation with a Ce^{3+} radius 1.778 (the default in *Gaussian03*), with the free energies of solvation from UATM with a Ce^{3+} radius of 1.523, indicate only a few kcal/mol difference. The B3LYP results that are based on UA0 and UAHF/UAKS cavities are consistent with the reported experimental values for the free energy of solvation of the cerium ion,[38,40] especially when water cluster models are considered and the small-core ECP is used on Ce^{3+}. Employing water clusters (reactions 6 and 8) leads to more negative free hydration energies than the models that involve discrete water molecules (reactions 7 and 9). The average value for reactions 6 and 8 with UA0 and UAHF/UAKS cavities and the small-core RECP is −780.08 kcal/mol with a standard deviation of 6.93, which is in excellent agreement with the experimental work of Gomer and Tryson (−786.3 kcal/mol), as well as Choppin (−774.2 ± 11 kcal/mol).[38,40] Individually, we observe that the UA0 cavity reproduces the Gomer and Tryson results within 3 kcal/mol depending on whether reaction 6 or 8 is used. In contrast, the UAHF/UAKS cavities yield results that are closer to the Choppin work and are also within 3−4 kcal/mol depending on whether reaction 6 or 8 is used. These results together with the calculated aqueous free energies of the reaction 1 suggest that cavities generated with UA0, UAHF, and UAKS radii in the PCM approach are most appropriate for aqua-cerium(III) ions when using only a primary hydration shell.

In comparison to the small-core thermodynamic values, those obtained using a large core have free energies of hydration are more positive by *ca*. 20 kcal/mol. This is interesting in light of the fact that employing a large-core RECP has little influence on the solvation interactions of $Ce(H_2O)_8^{3+}$ and $Ce(H_2O)_9^{3+}$ species because the metal is buried inside the complex. Moreover, only small differences in $\Delta\Delta G_{solv.}$ are observed between the small-core and large-core results (presumably caused by structural differences of the gas-phase optimized geometries), indicating that the variation in free energies of hydration may be attributable to the gas-phase thermochemistry results for reactions 6 and 8.

Performance of Density Functionals. As it is well-known that the nona-aqua Ce^{3+} species dominates in solution, we have further benchmarked the performance of LSDA (SVWN5), GGA (PW91), and meta-GGA (TPSS) functionals for reaction 8, using the recommended PCM cavities discussed above. As seen in Table 6, the range of $\Delta G_{hyd}(Ce^{3+})$ values calculated among all functionals is quite small (within 3 kcal/mol). Using the UA0 PCM cavity, the LSDA and hybrid functionals predict essentially the same $\Delta G_{hyd}(Ce^{3+})$ of nearly −789 kcal/mol, while the GGA and meta-GGA functionals predict values that are only 2 kcal/mol more exergonic (more negative). This agrees well with the Gomer and Tryson results of −786.3 kcal/mol.[38] Thus, all DFT functionals perform quite well in light of the experimental error, though the LSDA and hybrid functionals are in slightly better agreement (in contrast to the structural performance). The results for the UAKS cavities are closely aligned with the experimental values of Choppin[40] (−774.2 ± 11 kcal/mol) and are all within the experimental error. The same trend in energetics of each functional is observed, with the LSDA and hybrid results being 2−3 kcal/mol less exergonic than the GGA and meta-GGA functionals.

Inclusion of a Second Hydration Shell. On the basis of the work of Gutowski and Dixon,[30] we have further investigated water clusters bound to Ce^{3+} that include both the first and second solvation shells. Due to computational expense, only the B3LYP functional has been used for this series of reactions. As in the previous calculations, both water clusters (reactions 10 and 12) and discrete water molecules (reactions 11 and 13) have been used to assess the contribution of the second solvation shell to the free energy of hydration.

$$Ce^{3+}_{(gas)} + (H_2O)_{22(aq)} \rightarrow Ce(H_2O)_8(H_2O)^{3+}_{14\,(aq)} \quad (10)$$

$$Ce_{(gas)}{}^{3+} + 22H_2O_{(aq)} \rightarrow Ce(H_2O)_8(H_2O)_{14}{}^{3+}{}_{(aq)} \quad (11)$$

$$Ce_{(gas)}{}^{3+} + (H_2O)_{21(aq)} \rightarrow Ce(H_2O)_9(H_2O)_{12}{}^{3+}{}_{(aq)} \quad (12)$$

$$Ce_{(gas)}{}^{3+} + 21H_2O_{(aq)} \rightarrow Ce(H_2O)_9(H_2O)_{12}{}^{3+}{}_{(aq)} \quad (13)$$

Our approach for modeling the second hydration shell started with 16 water molecules in the second shell of the 8-coordinate species (two water molecules hydrogen-bonded to each water molecule from the first shell), but during the geometry optimization, two water molecules were pushed into the third shell, and therefore eliminated. The gas-phase calculations for the 8-coordinate species concluded with 14 water molecules in the second shell (i.e., $Ce(H_2O)_8(H_2O)_{14}{}^{3+}$). Similarly, for the 9-coordinate species we started with 18 water molecules in the second shell, but our gas-phase calculations indicated that only 12 water molecules can be accommodated in this shell. As seen in Table 1, in the small-core calculations, inclusion of a second solvation shell leads to shortening of the Ce−O(1) bonds and lengthening of the Ce−O(2) bonds, as labeled in Figure 1, which leads to better agreement with solid-state crystal structure information for nona-aqua Ce^{3+} ion. In the large-core calculation, addition of a second solvation shell leads to contraction of the Ce-(2) bonds by ∼0.04 Å and, in turn, significantly closer agreement with the small-core geometries. Both the small- and large-core structures for $Ce(H_2O)_8(H_2O)_{14}{}^{3+}$ and $Ce(H_2O)_9(H_2O)_{12}{}^{3+}$ are in reasonable agreement with the experiment, as reported by Rizkalla and Choppin.[40] Their review paper includes information on the hydration number of the second shell of the Ce(III) ion obtained by electrophoresis and diffusion measurements. The reported number of waters in the second hydraton shell is 12.8 at an average Ce-OH_2 bond distance of 4.51 Å. This compares well with the average calculated bond distance for the second shell waters in $Ce(H_2O)_8(H_2O)_{14}{}^{3+}$ of 4.68Å(RSC28)/4.69Å (RLC47) and in $Ce(H_2O)_9(H_2O)_{12}{}^{3+}$ of 4.74 Å (RSC28)/4.77Å (RLC47).

The calculated hydration free energies with PCM corrections for the reactions 10 and 12 are listed in Table 7 using the B3LYP functional, as our studies above indicate little functional dependence upon the thermodynamics (energetics for reactions 11 and 13 presented in Supporting Information). In general, the discrete water molecules approach employed for reactions 11 and 13 shows very large deviations from the experiment due to an inappropriate description of the entropy term. For reactions 10 and 12, several interesting trends are observed as a function of PCM cavity. First, as in our study of the ΔG_{hydr} using only the first hydration shell, we observe that UA0 yields the most negative free energies, followed by UAHF/UAKS, then Pauling, and finally UFF. Further, the same 20−30 kcal/mol discrepancy

TABLE 6: Free Energy of Ce^{3+} Hydration (kcal/mol) for Reaction 8 Using PCM[a] and Different Functionals with Small-Core RECPs and the aug-cc-PVDZ Basis Set

functional	ΔG (298.15 K)	$\Delta\Delta G_{solv}$ (elec.)	$\Delta\Delta G_{solv}$ (nonelec.)	$\Delta\Delta G_{solv}$ (tot.)	SS corr.	$\Delta G_{corr.}$	Expt.
			UA0				
SVWN5	−413.20	−372.23	−4.05	−376.28	−0.48	−789.96	−786.3[b]
PW91	−415.36	−372.89	−4.05	−376.94	−0.48	−792.78	−774.2[c]
B3LYP	−412.76	−372.20	−4.05	−376.26	−0.48	−789.49	
TPSS	−414.99	−372.36	−4.05	−376.41	−0.48	−791.88	
			UAKS				
SVWN5	−413.20	−361.85	−2.66	−364.51	−0.48	−778.19	
PW91	−415.36	−362.64	−2.66	−365.30	−0.48	−781.14	
B3LYP	−412.76	−362.03	−2.66	−364.70	−0.48	−777.93	
TPSS	−414.99	−362.24	−2.66	−364.90	−0.48	−780.37	

[a] PCM calculations were performed with *Gaussian03* code using the gas-phase optimized geometries of $Ce(H_2O)_9{}^{3+}$ and $(H_2O)_9$ with the corresponding functional. [b] ref 38. [c] ref 40.

TABLE 7: Free Energy of Ce^{3+} Hydration (kcal/mol) Using Two Hydration Shells in PCM[a] with Different Cavities, and with Different Gas-Phase Solvation Models (Reactions 10 and 12) at B3LYP Level with Large-Core RECPs for Ce and the aug-cc-PVDZ Basis for O and H

rxn	PCM cavity	ΔG (298.15 K)	$\Delta\Delta G_{solv}$ (electrostatic)	$\Delta\Delta G_{solv}$ (nonelec.)	$\Delta\Delta G_{solv}$ (tot.)	SS corr.	ΔG_{corr}	expt.
			B3LYP/RSC28/aug-cc-PVDZ Level					
10	UA0	−556.28	−252.50	−5.10	−257.60	−0.20	−814.08	−786.3[b]
12	UA0	−541.98	−258.73	−6.80	−265.53	−0.20	−807.71	−774.2[c]
10	UFF	−556.28	−230.1	6.87	−223.22	−0.20	−779.70	
12	UFF	−541.98	−231.77	4.63	−230.23	−0.20	−772.41	
10	UAHF, UAKS	−556.28	−246.12	−2.78	−250.61	−0.20	−807.09	
12	UAHF, UAKS	−541.98	−252.11	−5.51	−257.61	−0.20	−799.79	
10	Pauling, $\alpha = 1.1$	−556.28	−250.77	8.18	−242.58	−0.20	−799.06	
12	Pauling, $\alpha = 1.1$	−541.98	−255.51	8.02	−247.50	−0.20	−789.68	
			B3LYP/RLC47/aug-cc-PVDZ Level					
10	UA0	−527.59	−253.21	−4.13	−257.33	−0.20	−785.11	−786.3[b]
12	UA0	−521.98	−258.95	−5.75	−264.70	−0.20	−786.88	−774.2[c]
10	UFF	−527.59	−229.74	9.68	−220.06	−0.20	−747.84	
12	UFF	−521.98	−235.31	4.83	−230.48	−0.20	−752.66	
10	UAHF, UAKS	−527.59	−246.52	−1.31	−247.84	−0.20	−775.62	
12	UAHF, UAKS	−521.98	−252.15	−5.29	−257.43	−0.20	−779.61	
10	Pauling, $\alpha = 1.1$	−527.59	−251.14	9.41	−241.72	−0.20	−769.50	
12	Pauling, $\alpha = 1.1$	−521.98	−256.18	8.39	−247.79	−0.20	−769.97	

[a] PCM calculations were performed with *Gaussian03* code using the gas-phase optimized geometries of $Ce(H_2O)_8(H_2O)_{14}{}^{3+}$, $Ce(H_2O)_9(H_2O)_{12}{}^{3+}$, $(H_2O)_{22}$, and $(H_2O)_{21}$. [b] ref 38. [c] ref 40.

TABLE 8: Thermodynamic Properties (kcal/mol) of Reaction 14 in Gas-Phase and Aqueous Solution at PCM, B3LYP/RLC47/aug-cc-pVDZ Level

PCM cavity	ΔH (298.15 K)	ΔG (298.15 K)	$\Delta\Delta G_{solv}$ (elec.)	$\Delta\Delta G_{solv}$ (nonelec.)	$\Delta\Delta G_{solv}$ (tot.)	SS corr.	$\Delta G_{corr.}$
			Gas Phase				
	−6.61	−4.52					
			Solvent Phase				
UA0			3.09	−2.70	0.38	0	−4.14
UFF			3.28	−4.90	−1.61	0	−6.13
UAHF, UAKS			3.08	−4.11	−1.02	0	−5.54
Pauling, $\alpha = 1.1$			4.36	−1.61	2.75	0	−1.77

is observed between the values calculated by the RSC28 and RLC47 basis sets, with the RSC28 values being more negative. Finally, the addition of the second hydration shell consistently adds approximately −30 kcal/mol to the value of ΔG_{hydr}, relative to those values calculated with only a primary hydration shell. In combination, these three features lead to very different performance of the various PCM cavities when a second hydration shell is present. Specifically, for reactions 10 and 12, with a small-core Ce(III) basis, UFF and Pauling cavities yield ΔG_{hydr} values in closest agreement with experiment depending on whether reaction 10 or 12 is examined. UFF cavities yield values within 5 kcal/mol of both the Gomer and Tryson and Choppin values of −786.3 and −774.2 kcal/mol, respectively, while the Pauling results for reaction 12 is within 3 kcal/mol of the −786.3 value. In contrast, because the large-core basis predicts ΔG_{hydr} values that are 20−30 kcal/mol higher in energy (less negative), the UA0 and UAHF/UAKS cavities yield results that are in the best agreement with the experimental values.

The net result of the calculated ΔG_{hydr} study for reactions 6, 8, 10, and 12 thus indicate the following: (a) the trends in magnitude of ΔG_{hydr} as a function of PCM cavity do not follow the trend in cavity size, (b) the calculated ΔG_{hydr} for the small-core basis are consistently 20−30 kcal/mol more negative than that calculated by the large-core basis (this is independent of geometric differences calculated by the two bases and instead implies that the deviations derive from the gas-phase electronic energies), and (c) owing to the differences in the RSC28 and RLC47 values and the dependence of the ΔG_{hydr} upon the number of waters of hydration (first vs second shell), the performance of the various PCM cavities is not consistent and should be benchmarked on a system by system basis.

Water Exchange Reactions: Part II. On the basis of the benchmarking results for the hydration free energy of Ce(III), in terms of both functional and PCM cavity performance, the B3LYP functional in combination with either the UA0 or UAKS PCM cavities and the RSC28 Ce(III) basis should yield reasonable estimates of the free energy of reaction 1, which contains only the primary hydration shell. As seen in Table 4, this combination of method and cavities yield a ΔG value of approximately −4 kcal/mol. We have also examined the importance of including explicit second solvation shells on the water exchange reaction from the second shell to the first shell in reaction 14 using the RLC47 basis with the UA0 PCM cavity

$$Ce(H_2O)_8(H_2O)_{14}^{3+} \rightarrow Ce(H_2O)_9(H_2O)_{12}(H_2O)^{3+} \quad (14)$$

To keep the number of particles constant and avoid the standard state correction for water solvation, we have considered the product $Ce(H_2O)_9(H_2O)_{12}(H_2O)^{3+}$species with one-third shell water molecule. Table 8 contains the gas-phase energetics of reaction 14 and free energy contributions of bulk water solvent. In comparison to reaction 1, the gas-phase results of reaction 14 are less than half as exothermic. In fact, the gas-phase free energy of reaction 14 is much more similar to the solvent-phase corrected value of reaction 1. This result is not surprising, as the presence of the second solvation shell mimics much of the bulk water dielectric with the inner-sphere metal−water complex. In support of this statement, the solvent-corrected free energies of reaction 14 are very close to the gas-phase results, implying that solvation contributions for reaction 14 are almost negligible due to cancelation between product and reactant. The largest solvent contribution to the free energy of only 2.75 kcal/mol was obtained with partially scaled Pauling cavities, whereas UA0, UFF, and UAHF/UAKS solute cavities generated much smaller contributions. If only the gas-phase free energy of −4.52 kcal/mol is considered, the deviation from the solvent-corrected free energy of reaction 1 with UA0 and UAHF/UAKS solute cavities is smaller than 0.5 kcal/mol. These results suggest that inclusion of the second solvation shell in the gas phase can account for bulk solvent effects for the intramolecular exchange of one water molecule between the primary and second hydration spheres of the Ce^{3+} ion. Further, nearly identical results are obtained for both reactions 1 and 14 using the recommended UA0 and UAKS PCM cavities (as discussed above).

Conclusions

The aqueous chemistry of Ce(III) has been benchmarked in terms of both structural and thermodynamic data against varying density functionals, small- versus large-core RECPS, polarized continuum, and solvation reaction models. Ce(III) was chosen, as it is computationally the most simple trivalent Ln to study that contains lone f-electrons. The multiconfigurational character of the octa-aqua and nona-aqua Ce(III) was examined using CASSCF, which confirmed that the wave function is well-described using a single configuration. DFT studies show that imposition of symmetry yields several low-energy states but also potential high-energy doublet E states, and when using DFT, it is important to ensure that the lowest possible state is obtained (via orbital rotation, for example). When studying hydrated Ce(III) with only the first solvation shell, the meta-GGA TPSS functional yielded the best results relative to the average solution-phase Ce(III) data, while TPSS, PW91, and B3LYP performed well in comparison to crystal structure data. Inclusion of a second solvation shell improved the structural agreement in comparison to a variety of aqua Ce(II) crystal structures. After testing UA0, UFF, UAHF/UAKS, and Pauling polarized continuum model cavities, the UA0 and UAKS cavities were found to best reproduce experimental free energies of hydration, $\Delta G_{hyd}(Ce^{3+})$, when using a small-core Ce(III) basis and a single hydration shell. Using either UAKS or UA0, the calculated $\Delta G_{hyd}(Ce^{3+})$ was found to be insensitive to the density functional used, with all functionals performing equally well. In contrast, when a second hydration shell is employed the UFF and Pauling cavities are recommended with the small-core Ce(III) basis. In contrast to previous results, we found that the free energies of hydration did not correlate well to the size

of the cavity, and this work implies that cavity shape may be important for hard-sphere cations. The size of the relativistic effective core potential was found to dramatically influence calculated free energies of hydration, with the large-core results performing poorly. Inclusion of a second solvation shell improved the large-core results. Two different models of exchange reactions were considered for octa-aqua Ce(III) going to the nona-aqua species. The first was a simple addition reaction, while the second included migration of a second-shell water into the primary hydration sphere. Our best estimate for the free energy of CN = 8 to CN = 9 water exchange of Ce(III) is approximately −4 kcal/mol.

Acknowledgment. Work by A.D. was supported by the U.S. Department of Energy, INL Laboratory Directed Research & Development Program under DOE Idaho Operations Office Contract DE-AC07-05ID14517. A.E.C. recognizes support from the U.S. Department of Energy, Office of Nuclear Energy, Science and Technology, Junior Faculty Award Program award #DE-FG07-05ID14692/IDNE006. This research was performed in part using (1) the Molecular Science Computing Facility (MSCF) in the William R. Wiley Environmental Molecular Sciences Laboratory, a national scientific user facility sponsored by the U.S. Department of Energy Office of Biological and Environmental Research and located at the Pacific Northwest National Laboratory, operated for the Department of Energy by Battelle; (2) the National Energy Research Scientific Computing Center (NERSC) a DOE Office of Science user facility at Lawrence Berkely National Laboratory.

Supporting Information Available: Tables of Cartesian coordinates of all species and PCM cavity sizes. This material is available free of charge via the Internet at http://pubs.acs.org.

References and Notes

(1) Dhami, P. S.; Dudwadkar, N. L.; Achuthan, P. V.; Jambunathan, U.; Dey, P. K. *Sep. Sci. Technol.* **2004**, *39*, 3143.

(2) Salmon, P. S.; Neilson, G. W.; Enderby, J. E. *J. Phys. C.: Solid State Phys* **1988**, *21*, 1335.

(3) Clavaguera, C.; Gognon, J.-P.; Pyykko, P. *Chem. Phys. Lett.* **2006**, *429*, 8–12.

(4) Helm, L.; Merbach, A. E. *Coord. Chem. Rev.* **1999**, *187*, 151.

(5) Clavaguera, C.; Pollet, R.; Soudan, J. M.; Brenner, V.; Dognon, J.-P. *J. Phys. Chem. B* **2005**, *109*, 7614.

(6) (a) Clark, A. E. *J. Chem. Theor. Comput.* **2008**, *4*, 708. (b) Reed, A. E.; Weinstock, R. B.; Weinhold, F. *J. Chem. Phys.* **1985**, *83*, 735–746.

(7) Bylaska, W. A.; de Jong, K.; Kowalski, T. P.; Straatsma, M.; Valiev, D.; Wang, E.; Aprà, T. L.; Windus, S.; Hirata, M. T.; Hackler, Y.; Zhao, P.-D.; Fan, R. J.; Harrison, M.; Dupuis, D. M. A.; Smith, J.; Nieplocha, V.; Tipparaju, M.; Krishnan, A. A.; Auer, M.; Nooijen, E.; Brown, G.; Cisneros, G. I.; Fann, H.; Früchtl, J.; Garza, K.; Hirao, R.; Kendall, J. A.; Nichols, K.; Tsemekhman, K.; Wolinski, J.; Anchell, D.; Bernholdt, P.; Borowski, T.; Clark, D.; Clerc, H.; Dachsel, M.; Deegan, K.; Dyall, D.; Elwood, E.; Glendening, M.; Gutowski, A.; Hess, J.; Jaffe, B.; Johnson, J.; Ju, R.; Kobayashi, R.; Kutteh, Z.; Lin, R.; Littlefield, X.; Long, B.; Meng, T.; Nakajima, S.; Niu, L.; Pollack, M.; Rosing, G.; Sandrone, M.; Stave, H.; Taylor, G.; Thomas, J.; van Lenthe, A.; Zhang, Z. *NWChem, A Computational Chemistry Package for Parallel Computers*, version 5.0; Pacific Northwest National Laboratory; Richland, WA, 2006; pp 99352−0999.

(8) Frisch, M. J.; Trucks, G. W.; Schlegel, H. B.; Scuseria, G. E.; Robb, M. A.; Cheeseman, J. R. ; Montgomery J.A. Jr.; Vreven, T.; Kudin, K. N.; Burant, J.C.; Millam, J. M.; Iyengar, S. S.; Tomasi, J.; Barone, V.; Mennucci, B.; Cossi, M.; Scalmani, G.; Rega, N.; Petersson, G. A.; Nakatsuji, H.; Hada, M.; Ehara, M.; Toyota, K.; Fukuda, R.; Hasegawa, J.; Ishida, M.; Nakajima, T.; Honda, Y.; Kitao, O.; Nakai, H.; Klene, M.; Li, X.; Knox, J. E.; Hratchian, H. P.; Cross, J. B.; Bakken, V.; Adamo, C.; Jaramillo, J.; Gomperts, R.; Stratmann, R. E.; Yazyev, O.; Austin, A. J.; Cammi, R.; Pomelli, C.; Ochterski, J. W.; Ayala, P. Y.; Morokuma, K.; Voth, G. A.; Salvador, P.; Dannenberg, J. J.; Zakrzewski, V. G.; Dapprich, S.; Daniels, A. D.; Strain, M. C.; Farkas, O.; Malick, D. K.; Rabuck, A. D.; Raghavachari, K.; Foresman, J. B.; Ortiz, J. V.; Cui, Q.; Baboul, A. G.; Clifford, S.; Cioslowski, J.; Stefanov, B. B.; Liu, G.; Liashenko, A.; Piskorz, P.; Komaromi, I.; Martin, R. L.; Fox, D. J.; Keith, T.; Al.Laham, M. A.; Peng, C. Y.; Nanayakkara, A.; Challacombe, M.; Gill, P. M. W.; Johnson, B.; Chen, W.; Wong, M. W.; Gonzalez, C.; Pople, J. A. Gaussian 2003; Gaussian, Inc.: Wallingford, CT, 2004.

(9) (a) Becke, A. D. *J. Chem. Phys.* **1993**, *98*, 5648–5652. (b) Lee, C.; Yang, W.; Parr, R. G. *Phys. Rev. B* **1988**, *37*, 785–789.

(10) (a) Perdew, J. P.; SchmidtK. In*Density Functional Theory and Its Application to Materials*, Van Doren, V., Eds.; AIP Press: Melville, NY, 2001. (b) Mattsson, A E *Science* **2002**, *298*, 759.

(11) (a) Kohn, W.; Sham, L. *Phys. Rev.* **1965**, *A140*, 1133. (b) Vosko, S. H.; Wilk, L.; Nusair, M *Can. J. Phys* **1980**, *58*, 1200.

(12) Perdew, J. P.; Burke, K.; Wang, Y. *Phys. Rev. B* **1996**, *54*, 16533.

(13) Tao, J. M.; Perdew, J. P.; Staroverov, V. N.; Scuseria, G. E. *Phys. Rev. Lett.* **2003**, *91*, 146401.

(14) (a) Dolg, M.; Stoll, H.; Preuss, H. *J. Chem. Phys.* **1989**, *90*, 1730. (b) Cao, X.; Dolg, M. *THEOCHEM* **2002**, *581*, 139.

(15) (a) Dolg, M.; Stoll, H.; Savin, A.; Preuss, H. *Theor. Chim. Acta* **1989**, *75*, 173. (b) Dolg, M.; Stoll, H.; Preuss, H. *Theor. Chim. Acta* **1993**, *85*, 441.

(16) Dunning, T. H., Jr. *J. Chem. Phys.* **1989**, *90*, 1007.

(17) Moller, C.; Plesset, M. S. *Phys. Rev.* **1934**, *46*, 618.

(18) Roos, B. O. In *Ab Initio Methods in Quantum Chemsitry*; Lawley, K. P. , Ed.; Wiley: New York, 1987; Vol. 2, p 399.

(19) Boys, S. F.; Bernardi, F. *Mol. Phys.* **1970**, *19*, 553.

(20) Xantheas, S. S. *J. Chem. Phys.* **1996**, *104*, 8821.

(21) Tomasi, J.; Mennucci, B.; Cammi, R. *Chem. Rev.* **2005**, *105*, 2999.

(22) Barone, V.; Cossi, M.; Tomasi, J. *J. Chem. Phys.* **1997**, *107*, 3210.

(23) Pauling, L. *The Nature of the Chemical Bond*,3rd ed.; Cornell University Press: Ithaca, NY, 1960.

(24) Maron, L.; Eisenstein, O. *J. Phys. Chem. A* **2000**, *104*, 7140.

(25) (a) Harrowfield, J. M.; Kepert, D. L.; Patrick, J. M.; White, A. H. *Aust. J. Chem.* **1983**, *36*, 483. (b) Gerkin, R. E.; Reppart, W. J. *Acta Crystallogr., Sect. C: Cryst. Struct. Commun.* **1984**, *40*, 781. (c) Chatterjee, A.; Maslen, E. N.; Watson, K. J. *Acta Crystallogr., Sect. B: Struct. Sci.* **1988**, *44*, 381. (d) Dalgarno, S. J.; Raston, C. L. *J. Chem. Soc., Dalton Trans.* **2003**, 287. (e) Faithfull, D. L.; Harrowfield, J. M.; Ogden, M. I.; Skelton, B. W.; Third, K.; White, A. H. *Aust. J. Chem.* **1992**, *45*, 583. (f) Atwood, J. L.; Barbour, L. J.; Dalgarno, S. J.; Raston, C. L.; Webb, H. R. *J. Chem. Soc., Dalton Trans.* **2002**, 4351.

(26) Allen, P. G.; Bucher, J. J.; Shuh, D. K.; Edelstein, N. M.; Craig, I. *Inorg. Chem.* **2000**, *39*, 595.

(27) Gagliardi, L.; Cramer, C. J. *Inorg. Chem.* **2006**, *45*, 9442–9447.

(28) While the Kohn-Sham orbitals from DFT may be used to construct a single determinant wave- function, the orbitals themselves do contain an unknown amount of correlation.

(29) (a) Lowdin, P.-O. *J. Chem. Phys.* **1950**, *18*, 365. (b) Löwdin, P.-O. *Adv. Quantum Chem.* **1970**, *5*, 185. (c) Sanoyama, E.; Kobayashi, J.; Yaushita, S. *THEOCHEM* **1998**, *451*, 189.

(30) Gutowski, K. E.; Dixon, D. A. *J. Phys. Chem. A* **2006**, *110*, 8840.

(31) Martin, R. L.; Hay, P. J.; Pratt, L. R. *J. Phys. Chem. A* **1998**, *102*, 3565.

(32) (a) Zhan, C. G.; Dixon, D. A. *J. Phys. Chem. A* **2001**, *105*, 11534. (b) Zhan, C. G.; Dixon, D. A. *J. Phys. Chem. A* **2002**, *106*, 9737. (c) Zhan, C. G.; Dixon, D. A. *J. Phys. Chem. A* **2004**, *108*, 2020.

(33) Barone, V.; Cossi, M. *J. Phys. Chem. A* **1998**, *102*, 1995.

(34) Cosentino, O.; Villa, A.; Pitea, D.; Moro, G.; Barone, V. *J. Phys. Chem. B* **2000**, *104*, 8001.

(35) Tissandier, M D.; Cowen, K. A.; Feng, W. Y.; Gundlach, E.; Cohen, M. J.; Earhart, A. D.; Coe, J. V.; Tuttle, T. R, Jr *J. Phys. Chem. A* **1998**, *102*, 7787.

(36) Kelly, C. P.; Cramer, C. J.; Truhlar, D. G. *J. Phys. Chem. A* **2006**, *110*, 10478.

(37) Morss, R. L. *J. Phys. Chem.* **1971**, *75*, 392.

(38) Gomer, R.; Tryson, G. *J. Chem. Phys.* **1977**, *66*, 4413.

(39) Bratsch, S. G.; Lagowski, J. J. *J. Phys. Chem.* **1985**, *89*, 3317.

(40) (a) Rizkalla, E. N.; Choppin, G. R. Hydration and Hydrolysis of Lanthanides, In *Handbook of the Physics and Chemistry of Rare Earths*; Gschneider, K. A., Jr., Eyring, L., Eds.; 1991, Elsevier Science Publishers: Amsterdam; Vol *15*, pp 393−442; (b) pp 529−558.

JP8076408